JGR Atmospheres

RESEARCH ARTICLE
10.1029/2024JD042915

Observed Downdrafts and Ventilation During the Rapid Intensity Changes of Hurricane Delta (2020)

Nicholas E. Johnson[1], Brian H. Tang[1], Kristen L. Corbosiero[1], and Jonathan R. Moskaitis[2]

[1]Department of Atmospheric and Environmental Sciences, University at Albany, State University of New York, Albany, NY, USA, [2]U.S. Naval Research Laboratory, Monterey, CA, USA

Key Points:

- Downdraft ventilation, which can weaken tropical cyclones and complicate intensity forecasts, can be measured with aircraft observations
- Observations of Hurricane Delta showed deep, intense downdrafts and ventilation as rapid intensification ended and during rapid weakening
- The results of this observational study support the findings of previous modeling studies of downdraft ventilation

Correspondence to:

N. E. Johnson,
nejohnson@albany.edu

Citation:

Johnson, N. E., Tang, B. H., Corbosiero, K. L., & Moskaitis, J. R. (2025). Observed downdrafts and ventilation during the rapid intensity changes of Hurricane Delta (2020). *Journal of Geophysical Research: Atmospheres*, *130*, e2024JD042915. https://doi.org/10.1029/2024JD042915

Received 8 NOV 2024
Accepted 30 APR 2025

Abstract This study examines downdrafts and downdraft ventilation, and their effects on Hurricane Delta (2020). Delta experienced rapid intensification (RI) before abruptly weakening before making landfall. Two sampling periods by reconnaissance aircraft provided observations during RI and the subsequent rapid weakening, giving an opportunity to study the downdraft evolution and compare these two periods. Across both sampling periods, the vertical wind shear increased, causing the vortex to tilt and exposing Delta's inner core to the surrounding environment. The increased shear provided a pathway for downdraft ventilation, the transport of low-equivalent potential temperature (θ_e) air aloft into the boundary layer via downdrafts. Aircraft Doppler radar measured intense, deep downdrafts toward the end of the RI period; however, minimal downdraft ventilation was observed. After peak intensity, during the weakening period, downdraft ventilation was more prevalent with moderate to intense downdrafts and low-θ_e air concentrated on the left-of-tilt side of the storm. The observations show that as Delta weakened, the inner core became diluted with low-θ_e air from downdraft ventilation and the convection was limited to the downtilt and left-of-tilt regions of the storm. These findings are consistent with previous idealized and real-case modeling studies that have shown downdraft ventilation weakens tropical cyclones and degrades their structure. Additionally, the location of the downdraft ventilation observations relative to the vortex tilt and shear directions agree with previous modeling studies. More broadly, observations of the downdraft structure and diagnostics of downdraft ventilation may provide cues of subsequent intensity change in sheared storms.

Plain Language Summary This study examines the downward transport of cool and dry air by downdrafts, known as downdraft ventilation, in Hurricane Delta (2020). Delta had rapid intensity changes making it challenging to predict. Observations of the storm made by reconnaissance aircraft are used to investigate downdraft ventilation and associated changes in the storm's structure. The results show that downdrafts were intense as the storm was getting stronger; however, minimal downdraft ventilation was observed. As the storm weakened, more downdraft ventilation was observed and the storm structure began to deteriorate, consistent with the storm's weakening. Observations of downdraft ventilation may be useful for improving hurricane intensity predictions.

1. Introduction

Many processes negatively affect tropical cyclone (TC) intensity including vertical wind shear, downdrafts, and ventilation. These phenomena, together, have been explored in numerical modeling studies but have received less examination using observations. Observing these processes can potentially improve TC intensity forecasts that are essential for community preparation ahead of a landfalling storm.

Vertical wind shear is one of the major factors governing TC intensity change (DeMaria & Kaplan, 1994; Rios-Berrios et al., 2016a, 2016b; Ryglicki et al., 2018). Shear can inhibit intensification by disrupting the vertical alignment of the vortex (Jones, 1995). A TC with a vertically aligned vortex is more likely to intensify than a TC with a tilted vortex since an aligned vortex promotes near-surface convergence of absolute vorticity that, combined with latent heat release within a closed circulation, leads to vortex spinup (Rios-Berrios et al., 2018; Van Sang et al., 2008). An aligned vortex is associated with a more favorable environment for latent heat release since it promotes the recirculation of air parcels, which reduces the likelihood of dry air intrusions from the environment (Rios-Berrios et al., 2018). The ability of a TC vortex to remain aligned depends on the intensity and size of the TC's tangential wind field, as defined by the Rossby penetration depth, which can be used to quantify the strength of the vortex coupling (Hoskins et al., 1985; Jones, 1995). More intense tangential winds and a larger

tangential wind field promote stronger vertical coupling of the vortex. A stronger vortex coupling facilitates cyclonic precession that limits vortex tilting (Jones, 1995). Finocchio and Rios-Berrios (2021) showed, in idealized simulations, that intense TCs near the end of rapid intensification (RI) tended to weaken when exposed to vertical wind shear since these TCs have compact tangential wind fields resulting in weaker vortex coupling that makes them more susceptible to tilting (Jones, 1995).

Vertical wind shear produces a precipitation asymmetry where most precipitation occurs downshear and maximizes downshear left in the inner core (e.g., Rios-Berrios et al., 2024). As the precipitation is transported cyclonically from the downshear to upshear side, downstream of rainband convection, it falls into unsaturated air below to develop evaporatively cooled downdrafts (Alland et al., 2021a; Nguyen & Molinari, 2012; Riemer et al., 2010; Riemer & Montgomery, 2011). The location and strength of the downdrafts is associated with the vortex tilt, usually occurring cyclonically downstream from the tilt direction and being stronger with a larger tilt magnitude (Alland et al., 2021a). The most intense downdrafts are generally found in convective precipitation at low-to mid-levels where the vigorous overturning of the air inside the convection causes a wide distribution of vertical velocity intensity (Didlake & Houze, 2009). In contrast, stratiform precipitation is more often associated with weaker vertical velocity magnitudes (Didlake & Houze, 2009).

In addition to the evaporatively-cooled mechanism, downdrafts can form because of other processes. Descent can result from the intrusion of cool, dry air at middle and upper levels (Alland & Davis, 2022; Alland et al., 2021b; Fischer et al., 2023), shear-induced subsidence (Zawislak et al., 2016), and convergence of storm-relative inflow with the TC's upper-level outflow upshear (Dai et al., 2021). Additionally, downdrafts may form adjacent to an eyewall updraft as a forced response to the updraft. Intense, deep downdrafts with magnitudes greater than 10 m s^{-1} and depths greater than 8 km across the troposphere have been documented in previous observational studies of TCs (R. A. Black et al., 1994; M. L. Black et al., 2002). These downdrafts were observed in updraft-downdraft couplets where updrafts were located on the downshear side of the TC eyewall and downdrafts, mixed with narrower weaker updrafts, were located across the eye on the upshear side (R. A. Black et al., 1994; M. L. Black et al., 2002). In both studies, it was suggested that the intense, deep downdrafts were caused by moist symmetric instability initiated by precipitation loading.

Downdrafts can transport low-equivalent potential temperature (θ_e) air into the TC boundary layer via downdraft ventilation, which is detrimental to TC intensity and structure (Alland et al., 2021a; Powell, 1990; Riemer et al., 2010, 2013; Wadler et al., 2021; Yu et al., 2023; Zhang et al., 2013). Vertical wind shear and vortex tilt provide a pathway for environmental low-θ_e air to intrude into the TC inner core (Alland et al., 2021a, 2021b; Tang & Emanuel, 2010). Downdraft ventilation has been shown to occur left-of-shear and cyclonically downstream of the tilt direction (left-of-tilt) in the modeling study of Alland et al. (2021a). Another pathway for ventilation is radial ventilation, which is the dilution of high-θ_e air in the TC inner core with low-θ_e air intruding from the environment via storm-relative inflow (Alland et al., 2021b; Gu et al., 2015; Tang & Emanuel, 2010, 2012a; Tang et al., 2016, 2024). In this study, we focus on examining downdraft ventilation.

Ventilation acts as "anti-fuel" for the TC, inhibiting intensification (Tang & Emanuel, 2010) and increasing uncertainty with intensity forecasts (Zhang et al., 2013; D. Tao & Zhang, 2014). Downdraft ventilation inhibits intensification by reducing the buoyancy feeding eyewall convection (Alland et al., 2021a; Riemer et al., 2010), reducing the vertical mass flux and causing vortex spindown (Smith & Montgomery, 2015).

The negative effects of downdraft ventilation on TC intensity can potentially be offset by air-sea enthalpy fluxes that warm and moisten (i.e., "recover") the low-θ_e air transported into the boundary layer (Nguyen et al., 2019; Tang & Emanuel, 2012b; Wadler et al., 2021). The effectiveness of the recovery process depends on the location of downdraft ventilation relative to downstream eyewall updrafts. In an idealized modeling study, Wadler et al. (2021) showed that downdraft ventilation is most detrimental to TC intensity when low-θ_e air is deposited into the top of the inflow layer within about 5 km from an eyewall updraft. In this situation, the low-θ_e air is too far from the sea surface and has minimal residence time in the boundary layer, which limits the ability of surface fluxes to recover the air. In contrast, Wadler et al. (2021) found that downdraft ventilation located more than about 10 km from an eyewall updraft has a limited effect on the TC intensity since parcels have more time to recover via surface fluxes before becoming entrained in the updraft.

The strength of the surface heat fluxes is influenced by the low-level environmental flow that enhances the surface fluxes to the right of the environmental flow direction, where surface winds are maximized, and reduces them to

the left (Chen et al., 2019; Rappin & Nolan, 2012). Additionally, the environmental flow can transport higher-θ_e air downstream, which enhances the recovery process there (Lee et al., 2021). The recovery process can be limited in cases of strong downdraft ventilation. Finocchio and Rios-Berrios (2021) found that intense TCs nearing the end of RI generally experience the strongest downdraft ventilation in response to increasing vertical wind shear. The downdraft ventilation in their RI case was strong enough to negate the recovery of the low-θ_e air by surface heat fluxes leading to weakening. As we will show, Hurricane Delta (2020) fits this situation where downdraft ventilation was observed toward the end of RI and after RI.

We seek to document downdraft ventilation measured from observations, adding to our understanding of downdraft ventilation based on previous modeling experiments. Since ventilation has primarily been examined in modeling studies, this study will help expand our knowledge of how ventilation manifests in a real TC. Measuring ventilation is challenging since it requires both wind and thermodynamic measurements. Hurricane Delta provides an excellent case to study downdraft ventilation using observations. Two aerial reconnaissance missions were flown in Delta during its rapid intensity changes. The first flight occurred shortly before Delta's peak intensity toward the end of RI, and the second flight was after peak intensity during rapid weakening. These flights were part of the Office of Naval Research (ONR) Tropical Cyclone Rapid Intensification (TCRI) field campaign, which provided more dropsonde observations than a typical reconnaissance flight. The increased number of dropsonde observations and the timing in relation to Delta's intensity evolution make the storm an ideal candidate for investigating ventilation.

In this study, we utilize dropsonde observations to calculate downdraft ventilation in Hurricane Delta and compare it with tail Doppler radar (TDR) observations of the larger-scale TC structure. There have been a few observational studies of downdraft ventilation where the vertical velocity observations used in the analyses were measured by the TDR (e.g., Nguyen et al., 2017; Wadler et al., 2018). However, to the authors' knowledge, this is the first study to consider downdraft ventilation using vertical velocity estimates directly from dropsondes. The dropsonde vertical velocity measurements have a higher vertical resolution than the TDR and coincide with dropsonde thermodynamic measurements needed to quantify ventilation.

The goals of this study are to: (a) Demonstrate a method for measuring downdraft ventilation from dropsonde observations; (b) link observations of θ_e, vertical motion, and convective features in Hurricane Delta (2020) to its intensity changes; and, (c) compare observations of downdraft ventilation with the results of previous modeling studies. Section 2 provides an overview of Delta during the period of analysis. Section 3 presents the methods employed to measure downdrafts and downdraft ventilation. Section 4 describes the observations of intense, deep downdrafts and downdraft ventilation in Delta during two aerial reconnaissance flights. Section 5 discusses potential causes for the intense, deep downdrafts. Section 6 discusses the connection between the results and Delta's intensity changes, and compares the results with previous studies.

2. Synopsis of Hurricane Delta

Hurricane Delta (2020) had an interesting intensity forecast evolution due to rapid changes in the TC's structure and environmental conditions, making it challenging to predict. The evolution of Delta from its formation until landfall is shown in Figure 1. The TC formed in the Caribbean Sea, south of Jamaica, on 4 October 2020 and attained tropical storm intensity 18 hr later. Over the next 36 hr, Delta moved northwest toward the Yucatán Peninsula and rapidly intensified to 120 kt. This strengthening marked one of the fastest intensifications on record of an Atlantic TC. After reaching peak intensity, Delta abruptly and rapidly weakened to 90 kt before making landfall on the Yucatán Peninsula (Cangialosi & Berg, 2021). The rapid weakening was unexpected and intensity forecasts from the National Hurricane Center (NHC) with a 12-hr lead time predicted Delta would continue to intensify before making landfall (Figure 1).

During Delta's RI period, the TC had a compact inner core with a radius of maximum wind (RMW) of 15 km estimated from tail Doppler radar (see Methods). The inner core was marked by very cold IR brightness temperatures indicating deep convection (Figure 1). When Delta began weakening, the RMW increased to 28 km and the central dense overcast expanded radially outward (Figure 1).

Between Delta's RI and weakening periods, the vertical wind shear and vortex tilt increased. Toward the end of RI, the vertical wind shear near Delta was 6 m s^{-1}, in the moderate range (Rios-Berrios & Torn, 2017). Additionally, Delta's 0–6-km vortex tilt was 10 km. As Delta was weakening, the shear increased to 9 m s^{-1} and the

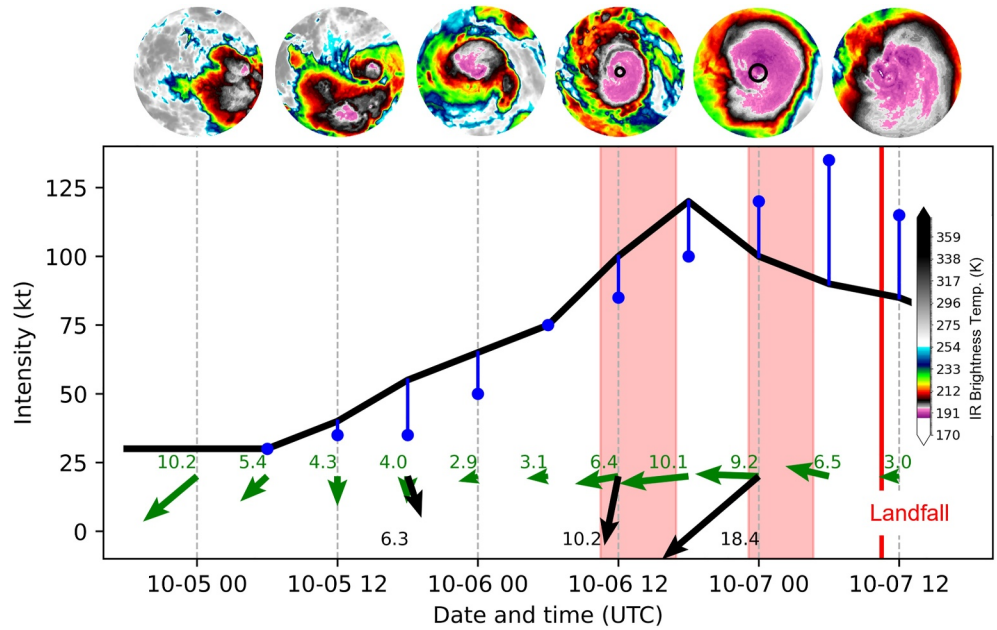

Figure 1. Best track intensity time series of Hurricane Delta from 1800 UTC 04 Oct 2020 to 1200 UTC 07 Oct 2020. Red shaded regions indicate P-3 dropsonde sampling periods of interest. Snapshots of infrared (IR) satellite imagery, centered on the storm over a 2° radius disc, are shown in 12-hr increments along the top of the figure. Black circles on the IR images during flights show the RMW measured by the TDR at 2-km height. The 850–200-hPa shear vector and magnitude $(\mathrm{m\ s^{-1}})$, from the Statistical Hurricane Intensity Prediction Scheme (SHIPS) developmental database, are shown in green in 6-hr increments along the bottom of the figure. The 0–6-km vortex tilt vector and magnitude (km) measured by the TDR during each P-3 flight are shown in black at the bottom of the figure. Blue points indicate the 12-hr NHC forecasts and the blue lines indicate the corresponding error. The red line marks the landfall time.

vortex tilt increased to 18 km. The cause of the shear increase was associated with an upper-level anticyclone southeast of Florida and northeast of Delta (not shown). Figure 2 shows a streamline analysis from the TDR during both reconnaissance flights highlighting the vortex tilt. Comparing the two TDR analyses, the mid-level center, indicated by the 6-km streamlines, became displaced to the southwest from the low-level center, marked by the 2-km streamlines. The misalignment of the mid- and low-level centers potentially provides increased exposure of the TC vortex to the surrounding environment. Particularly on the left-of-tilt (eastern) side of the TC,

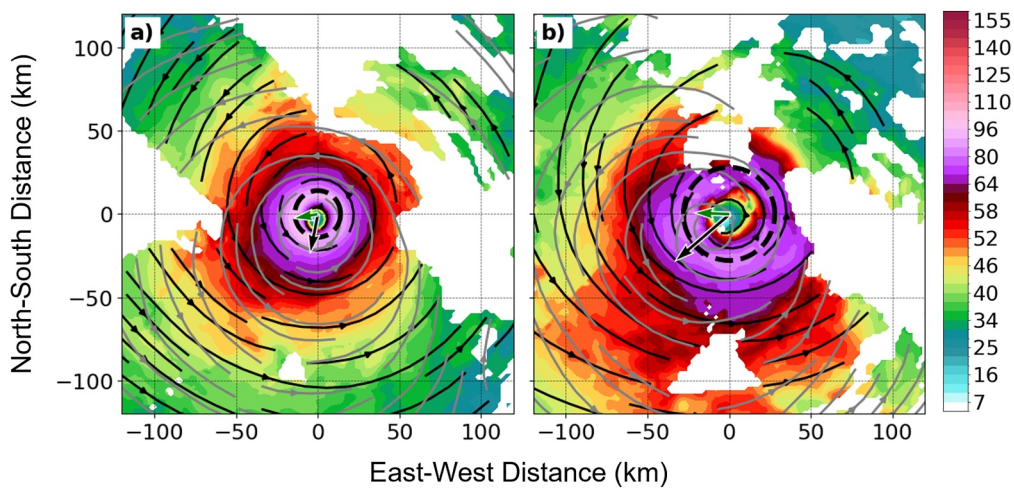

Figure 2. TDR 2-km wind speed (kt, shading) and streamlines at 2 km (black) and 6 km (gray) during (a) flight 1 and (b) flight 2. The black and green arrows indicate the tilt and shear directions, respectively. Note that the vectors are not scaled with the plot axes. The dashed black circle is the RMW.

the 6-km streamlines crossing inward over the 2-km streamlines is indicative of relatively low-θ_e, dry air (not shown) intruding from the environment toward the inner core (e.g., Tang et al., 2024).

3. Methods

3.1. TDR and Dropsonde Overview

Hurricane Delta's evolution during its periods of rapid intensity change is examined using observations collected by two National Oceanic and Atmospheric Administration (NOAA) WP-3D (P-3) reconnaissance flights. The time of both flights in relation to Delta's intensity is shown in Figure 1. The structure of the TC and downdraft ventilation are diagnosed using a combination of measurements from the TDR and dropsondes. Specifically, wind and reflectivity measurements from the TDR are used to examine downdrafts and TC structure, and dropsondes are used to study the lower-tropospheric downdraft ventilation in the TC inner core. Vertical wind shear information is acquired from the Statistical Hurricane Intensity Prediction Scheme (SHIPS) developmental database.

Analyses in this study that use the TDR rely on the Tropical Cyclone Radar Archive of Doppler Analyses with Recentering (TC-RADAR) analyses (Fischer et al., 2022) and TDR vertical profile data sets (Lorsolo et al., 2010; Zhang et al., 2023).

The TC-RADAR data set provides three-dimensional analyses of TDR data with 2-km horizontal resolution and 500-m vertical resolution. The radar observations are available out to a horizontal distance of approximately 50 km from the aircraft, which is sufficient for our analysis of downdraft ventilation in Delta. RMW and vortex tilt information were acquired from merged analyses that combine all TDR observations during a flight. The TDR fields, however, are taken from the individual swath analyses of each center pass to examine the convective-scale features of Delta that changed rapidly between each pass. The TC-RADAR analyses include radar fields that are mapped to a storm-centered grid following a center-finding technique described by Fischer et al. (2022). The vertical wind field in TC-RADAR is calculated using a variational technique that employs the mass continuity and radar projection equations (Gamache, 1997; Gao et al., 1999; Reasor et al., 2009). This vertical wind calculation could result in smoothing of smaller scale features (Fischer et al., 2022).

The TDR profile data set, developed using a method described by Zhang et al. (2023), offers an alternative to the TC-RADAR vertical wind field. The profiles are generated without the mass continuity equation with a vertical resolution of 150 m that reduces smoothing and helps resolve smaller-scale features. The profiles are only available along the aircraft flight track in a two-dimensional plane with radius and height coordinates.

In addition to TDR observations, thermodynamic and wind measurements from dropsondes are used to quantify downdraft ventilation. Quality-controlled dropsonde data were obtained from NOAA. During both flights used in this study, the aircraft flew at a constant pressure of 700 hPa so the dropsonde profiles generally extend from the surface to just above 3-km height.

To facilitate analyses in this study that combine dropsonde and TDR swath observations, both data sets were transformed into a storm-centered cylindrical framework. The TC center defining the cylindrical grid was based on the 2-min TC position estimates from NOAA, which are determined from flight-level wind center fixes around 3-km height using the methods descried by Willoughby and Chelmow (1982). Dropsondes were converted to the cylindrical framework by matching the time and location of each dropsonde measurement to the closest-in-time center location, which allowed the dropsonde observations to be compared as if they were collected instantaneously. Additionally, the dropsonde data were mapped to a consistent altitude grid with 5-m vertical spacing. For Delta specifically, the storm-centered grid provided in the TC-RADAR data set was slightly offset from the subjective center determined from the reflectivity and horizontal wind measurements. For consistency, the storm-relative grid for the TDR swath analyses in Delta was recalculated using the TC center retrieved from the 2-min TC position estimates used to transform the dropsonde data. The TDR analyses were transformed into the cylindrical framework using the methods of Ahern and Cowan (2018).

3.2. Precipitation Partitioning

A precipitation partitioning algorithm was employed to determine the precipitation mode near Delta's center based on the TDR reflectivity observations. The precipitation modes are categorized as weak echo, stratiform, shallow convection, moderate convection, or deep convection. The algorithm was first described by Churchill and

Houze (1984) and has been applied to ground-based radar (Alvey et al., 2022; Steiner et al., 1995), airborne radar (Didlake & Houze, 2009; Rogers et al., 2020; Wadler et al., 2023), and satellite radar (C. Tao & Jiang, 2015). Weak echoes are categorized where reflectivity at 2-km height is less than 15 dBZ. Precipitation is categorized as convection in two ways: Either where the 2-km reflectivity is greater than 35 dBZ or where the reflectivity is greater than the convective center criterion from Yuter and Houze (1997). The convective center criterion is a function of the area average background reflectivity within an 11-km-radius disc and empirical tuning coefficients that are defined in several studies (Didlake & Houze, 2009; Rogers et al., 2020; Wadler et al., 2023). All grid points that are not classified as weak or convective are labeled stratiform. The depth of the convective precipitation was determined by the height of the 20-dBZ echo top (Rogers et al., 2020; Wadler et al., 2023). Convection is categorized as shallow when the 20-dBZ echo top is at or below 6 km, moderate when the top is between 6 and 10 km, and deep when it is above 10 km. To account for calibration differences between the radar systems on the two NOAA P-3 aircraft, bias-corrected TC-RADAR reflectivity data developed by Wadler et al. (2023) is used when calculating the precipitation modes.

3.3. Downdraft Ventilation Calculation

Downdraft ventilation is quantified by calculating the downward flux of perturbation θ_e:

$$w_{\downarrow}\theta'_e \tag{1}$$

where $w_{\downarrow}$ is the downward (negative) vertical wind and θ'_e is the perturbation equivalent potential temperature from the azimuthal mean (Riemer et al., 2010). Downdraft ventilation, the downward transport of below-mean-θ_e air, has positive values by this formula.

The azimuthal mean θ_e is estimated by finding the average θ_e profile from all the dropsondes launched within 2x the RMW, not including the eye, during each flight. This calculation assumes that the observations were collected instantaneously, which was necessary to gain sufficient azimuthal coverage. To offset the nonuniform spatial distribution of the dropsondes, we binned the observations by shear quadrant accounting for the horizontal drift as the dropsonde falls, averaging first within each quadrant and then averaging the quadrants together, following Tang et al. (2024). One limitation of this method for estimating the azimuthal-mean θ_e is the availability of dropsonde observations in all quadrants of the TC. During the first flight, there were no dropsonde observations in the downshear-right quadrant below 500 m due to dropsonde drift, so the azimuthal average estimate below 500 m does not include that quadrant. The increased number of dropsondes per flight, available through the TCRI project, helped with the azimuthal average estimate. The azimuthal average calculation for the first flight included nine dropsondes and the calculation for the second flight included 16 dropsondes.

The dropsonde vertical wind, provided in the dropsonde data sets, was calculated by comparing the dropsonde fall rate to the theoretical fall rate of a dropsonde in a quiescent environment (Franklin et al., 2003). Franklin et al. (2003) suggested that the absolute uncertainty of the dropsonde vertical wind is about 0.5–1.0 m s^{-1}. Stern et al. (2016) performed an analysis of the uncertainty in the vertical wind estimation that resulted from differences in the dropsonde mass and parachute size. They found that, by varying the parameters, the uncertainty of the vertical wind estimates was around 1 m s^{-1} in the lower troposphere. Furthermore, Wang et al. (2009) used the same method to estimate vertical wind from dropsondes and similarly found that the accuracy of the estimates improved for vertical wind magnitudes greater than 1 m s^{-1}. The uncertainty in estimating the vertical wind would be problematic for diagnosing downdraft ventilation in weak downdrafts; however, as will be seen, many of the downdrafts sampled in Delta were much stronger than 1 m s^{-1}. Additionally, a comparison between dropsonde vertical wind and TDR vertical wind showed general agreement between the two platforms (not shown).

4. Results

4.1. Flight 1: RI Period

Since Delta was undergoing RI, one might expect strong and symmetric upward motion in the eyewall; however, this is not the case. Figure 3 shows TDR profiles of vertical wind from four passes through the TC center during flight 1. There were pronounced asymmetries in the vertical motion in the eyewall where deep updrafts were

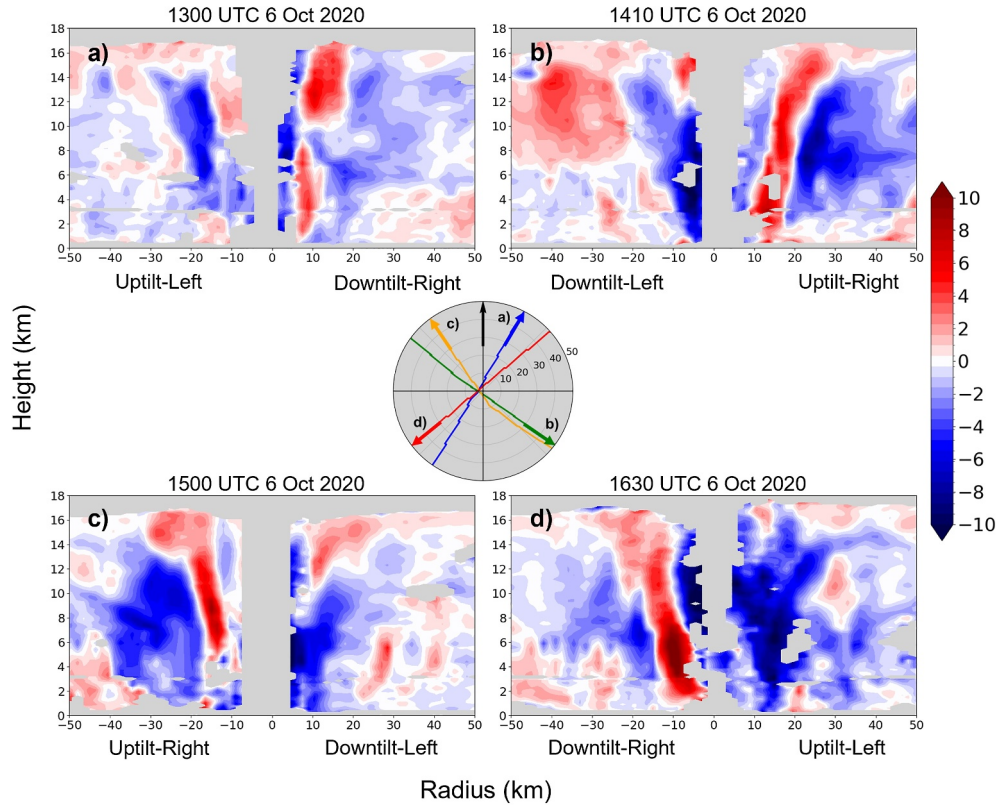

Figure 3. Radius-height profiles of vertical wind $\left(\mathrm{m\ s^{-1}}\right)$ along the aircraft flight track across four passes through the center of Hurricane Delta (2020) measured by the TDR on a NOAA P-3 aircraft. The time and tilt quadrants are labeled for each panel. The polar plot shows the flight track and direction for each profile with the tilt direction marked by the black arrow.

confined mostly right-of-tilt while, surprisingly, there were intense, deep downdrafts mostly left-of-tilt. Some of these downdrafts extended from the surface up to 12-km height. Over the 5 hours sampled by the TDR profiles, the depth of the downdrafts remained about the same. However, the intensity of the downdrafts in the uptilt-left quadrant doubled from about -5 to -10 m s^{-1} as the TC was nearing its peak intensity toward the end of the sampling period (Figures 3a and 3d). The updrafts extended to the top of the TDR profiles around 16 km and, like the downdrafts, maintained the same depth over the sampling period. The intense, deep downdrafts during the RI period are examined in more detail in Section 5.

To investigate whether ventilation occurred with the intense downdrafts, dropsonde observations were examined. All the inner core dropsondes were launched within 30 km of the TC center (~2x the RMW). Observations of downdraft ventilation and its components are shown in Figure 4 at 500-m height to examine ventilation in the boundary layer where previous studies have shown it is more likely to affect TC intensity (e.g., Riemer et al., 2010; Wadler et al., 2021). Downward motion was measured by most of the dropsondes at 500 m with a few measuring downdrafts <-5 m s^{-1} (Figure 4a). The downdrafts were predominantly located left-of-tilt, which matches the azimuthal location of the downdrafts observed by the TDR in Figure 3. θ_e mostly exceeded 360 K at 500 m with an average θ_e of 363 K for all the inner core dropsondes (Figure 4b). Six of the inner-core dropsondes measured below-mean θ_e collocated with downward motion below 1-km height. The resulting downdraft ventilation magnitudes (Figure 4c) were mostly less than 5 K m s^{-1} at 500 m.

Profiles of θ_e, vertical wind, and downdraft ventilation from five dropsondes are shown in Figure 5 (corresponding to points with bold outlines and capital letters in Figure 4, with the exception of dropsonde F, which is discussed later). Dropsondes A and B have downdraft ventilation magnitudes less than about 10 K m s^{-1} below 500 m (Figures 5k and 5l), corresponding to the small negative θ_e perturbations (Figures 5a and 5b) and moderate to intense downdrafts (Figures 5f and 5g) at those levels. Dropsondes C and E measured deeper layers of moderate to intense downdrafts (Figures 5h and 5j), but little in the way of downdraft ventilation (Figures 5m and 5o) due to

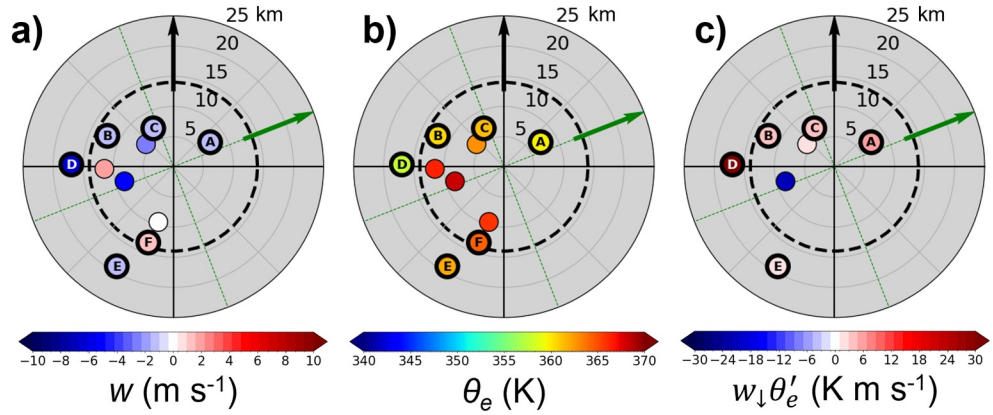

Figure 4. (a) Vertical velocity $\left(\text{m s}^{-1}\right)$, (b) θ_e (K), and (c) downdraft ventilation ($w_{\downarrow}\theta_e'$; K m s^{-1}; only where $w < 0$) measured by all dropsondes launched from a NOAA P-3 aircraft within 2x RMW, not including the eye, in Hurricane Delta (2020) at 500-m height from 1030 to 1700 UTC 6 Oct 2020. Points with letters and bold outlines indicate dropsondes that are discussed in following figures. The black and green arrows indicate the tilt and shear directions, respectively. The dashed back circle marks the RMW. Dropsonde F does not appear in panel c since downdraft ventilation was not observed due to the dropsonde measuring upward motion.

small θ_e perturbations (Figures 5c and 5e). Of all the dropsondes launched during this sampling period, dropsonde D measured the largest downdraft ventilation over the deepest layer from 1.5 km to the surface (Figure 5n). Dropsonde D had a negative θ_e perturbation for most of the profile with the most negative θ_e' below about 500 m (Figure 5d). This negative θ_e perturbation combined with intense downward motion, as large as -9 m s^{-1} over the lowest 1.5 km of the profile (Figure 5i), resulted in a deeper layer of more substantial downdraft ventilation. The downdraft ventilation observed by dropsonde D occurred during the last center pass of flight 1 about 1.5 hr before Delta reached peak intensity.

Because of the inherent sparseness of the dropsonde observations, the negative θ_e perturbation measured by dropsonde D could be related to the sharp radial gradient of θ_e typically seen outside TC eyewalls. However, based on the available observations, it appears that the θ_e measured by dropsonde D was indeed anomalously low. Dropsonde E was farther from the center than dropsonde D but measured greater θ_e. Furthermore, dropsonde F was at a similar radius as dropsonde D and also had larger θ_e.

The connection between the downdraft ventilation observations and the TC structure was examined by comparing the dropsonde and TDR observations (Figures 6 and 7). The observations in Figure 6 are shown at 2.5-km height to connect the near-center convective features above the boundary layer with the dropsonde measurements, and since the TDR observations are more reliable above 500 m. During four center passes, the largest reflectivity, between 40 and 50 dBZ, was located primarily downtilt and left-of-shear. The TDR-measured downdrafts were primarily located left-of-tilt and upshear. During three of the four passes (Figures 6a and 6d), the TC eye can be seen as the low reflectivity region near the center with a radius of about 5 km. Figure 7 shows the precipitation types, and highlights the dropsonde downdraft ventilation at 500-m to connect the ventilation observations with the precipitation structure and cloud types. Deep convection mostly surrounded the TC center (Figure 7). Four of the five dropsondes that measured downdraft ventilation (dropsondes A–D) during these passes were in convective precipitation (Figure 7).

Dropsondes A, B, and C were located between 6 and 13 km from the TC center right-of-tilt and downtilt (Figures 6a–6c). The three dropsondes were in moderate to deep convective precipitation for almost the entirety of their tracks (Figures 7a–7c). The top of the profile from dropsonde A, where low θ_e was measured, was located just outside the convection in stratiform precipitation (Figure 7a). As dropsonde A moved into the convective precipitation, the θ_e increased by nearly 15 K (Figures 5a and 7a). The three dropsondes measured small downdraft ventilation below 500 m in the downtilt semicircle in areas of moderate reflectivity around 35 dBZ (Figures 6a–6c).

Dropsonde D, which measured the largest downdraft ventilation, was located mostly downtilt-left between 7 and 17 km from the TC center (Figure 6d). The top of the profile was in an updraft measured by both the TDR and

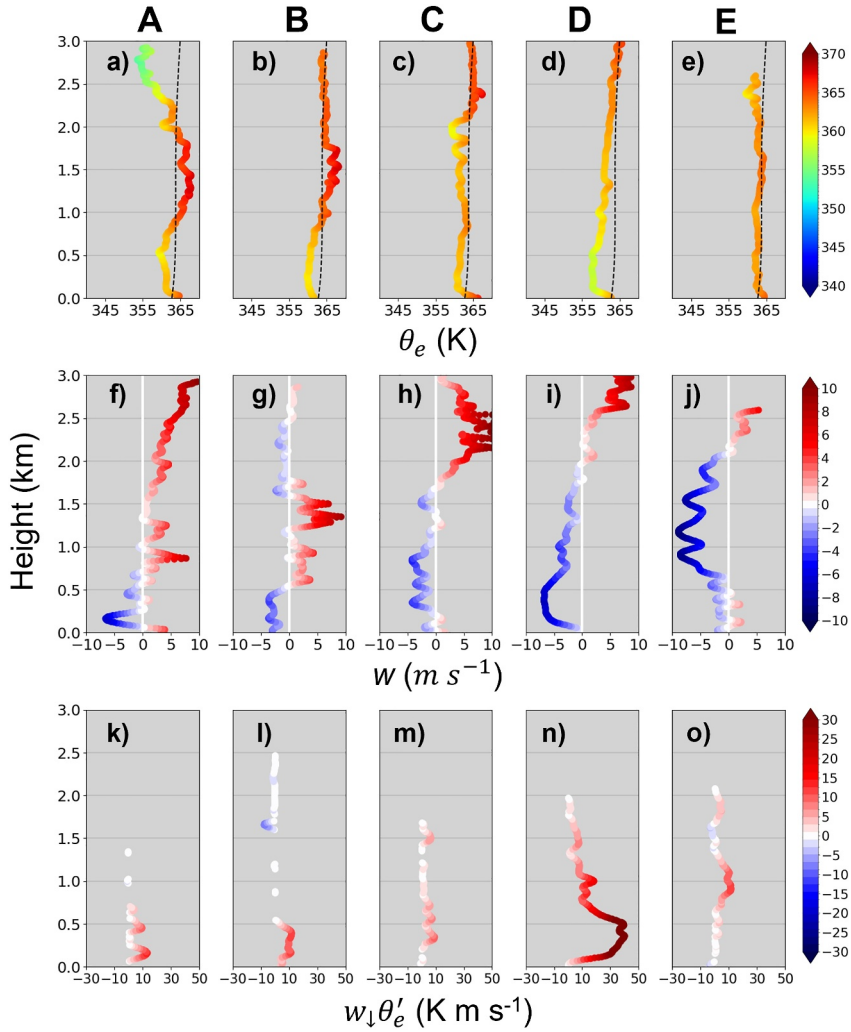

Figure 5. Profiles of θ_e (K; top row), vertical wind (m s^{-1}; middle row), and downdraft ventilation ($w_{\downarrow}\theta_e'$; K m s^{-1}; bottom row) measured by five individual dropsondes where downdraft ventilation was observed during flight 1 (see bold dots in Figure 4). Each column, indicated by capital letters (corresponding to Figure 4), is the same dropsonde. The black, dashed line in panels (a–e) indicates the mean θ_e profile.

dropsonde (Figures 5i and 6d). The dropsonde fell into a downdraft located left-of-tilt where greater downdraft ventilation was measured. Throughout the profile, the dropsonde was in deep convective precipitation and moderate reflectivity near 35 dBZ (Figures 6d and 7d). The dropsonde fell along the interface between deep convection and a stratiform precipitation area with weaker reflectivity (Figures 6d and 7d).

Dropsonde E was located farther from the center at a radius of 18 km in the uptilt-left quadrant (Figure 6d). It was located completely in stratiform precipitation outside the convective precipitation area (Figure 7d). Despite the different precipitation mode, dropsonde E still measured large θ_e near 365 K like the other dropsondes (Figures 5 and 6). The largest downdraft ventilation was measured near 1-km height where the downdraft was the most intense (around −9 m s^{-1}).

The deep, intense downdrafts point to a transitioning structure of the TC as it was nearing the end of RI. Despite the presence of these downdrafts, downdraft ventilation was isolated since θ_e was still large and asymmetries in θ_e from environmental intrusions had not yet fully developed. The few weak-to-moderate downdraft ventilation observations during the sampling period likely point to the initial development of downdraft ventilation in the TC, heralding the weakening that was about the commence. The next section discusses a similar analysis of the downdraft structure and downdraft ventilation during the second flight.

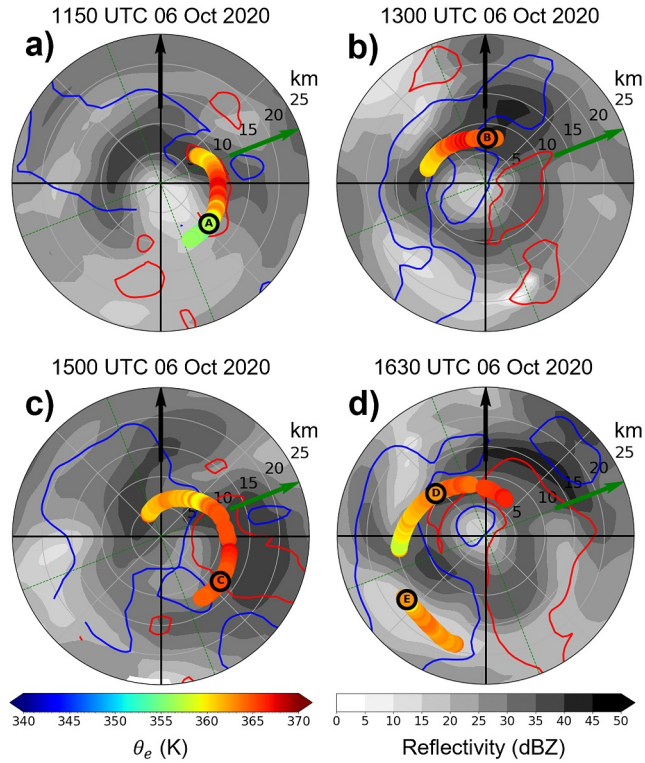

Figure 6. TDR reflectivity (dBZ, gray shading) and TDR vertical wind (m s^{-1}, contours) at 2.5 km during four NOAA P-3 passes through the center of Hurricane Delta from 1115 to 1655 UTC 6 Oct 2020. Red contours indicate +2 m s^{-1} vertical wind and blue contours indicate −1 m s^{-1} vertical wind. Colored dots are dropsonde θ_e (K) profiles. Colored points with black outlines show the θ_e measurement at 2.5 km with the letters corresponding to the dropsonde profiles in Figure 4. The black and green arrows indicate the tilt and shear directions, respectively.

4.2. Flight 2: Weakening Period

During the weakening period (Figure 1), the inner-core structure of Delta became much more disorganized. The vortex tilt increased to 18 km and the RMW increased to 28 km as the vertical wind shear increased to 9 m s^{-1}. Deep downdrafts continued to be observed in the TDR profiles. The along-tilt TDR profiles (Figures 8b and 8d) show the most intense downdrafts on the uptilt side of the TC. The downdrafts were located across the eye from intense updrafts on the downtilt side. The eyewall updrafts were located at larger radii compared to the first flight, consistent with the increase in the RMW. The across-tilt TDR profiles (Figures 8a and 8c) show downdrafts on both sides of the vortex at midlevels. TDR profile data were sparse uptilt and right-of-tilt in the lower levels, due to a lack of scatterers (not shown), so the extent of the downdrafts closer to the surface in these locations cannot be determined with the TDR. Dropsonde observations can help fill in some of these gaps.

We examined dropsonde observations within 60 km radius, about 2x the RMW, excluding observations within the eye. In the lowest 1 km, downward motion was measured in all four tilt quadrants with the most intense downdrafts (<−5 m s^{-1}) in the left-of-tilt and left-of-shear semicircles (Figure 9a).

Evidence of downdraft ventilation was observed by the majority of dropsondes on the left-of-tilt side during this period. Low-θ_e air existed close to Delta's center at 500 m with magnitudes as low as 350 K (Figure 9b). At 500-m height, the average dropsonde θ_e in the inner core (within 2x the RMW, not including the eye) was 357 K, 6 K less than during the RI period, although these observations cover a larger area compared to the previous flight. This change in θ_e indicates an overall decrease in the moist entropy of the TC inner core over the 12 hr between the two flights. Large values of downdraft ventilation were found in the left-of-tilt semicircle (Figure 9c) where the most intense downdrafts and lowest θ_e were observed. The decrease of θ_e in the inner core is consistent with the diluting effects of downdraft ventilation, where large quantities of low-θ_e air intrude into the boundary layer and weaken the TC.

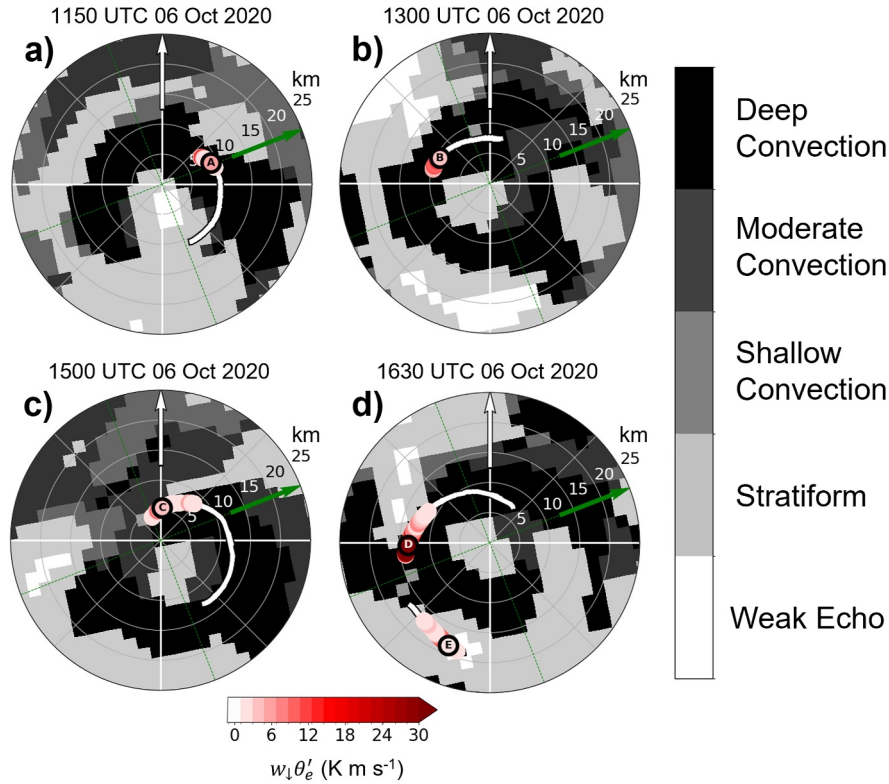

Figure 7. TDR precipitation type (gray shading) during four NOAA P-3 passes through the center of Hurricane Delta from 1115 to 1655 UTC 6 Oct 2020. Colored dots are dropsonde downdraft ventilation $\left(\text{K m s}^{-1}\right)$ greater than 1 K m s^{-1}. Colored points with black outlines show the downdraft ventilation measurement at 500 m with the letters corresponding to the dropsonde profiles in Figure 4. The white and green arrows indicate the tilt and shear directions, respectively.

4.2.1. Vertical Structure of Downdraft Ventilation

Profiles of θ_e, vertical wind, and downdraft ventilation (Figure 10) are now examined from five dropsondes on the left-of-tilt side identified in Figure 9 (points with bold outlines and capital letters). The dropsondes measured lower θ_e and deeper layers of negative θ_e perturbations compared to the RI period. The downward motion was mostly between −2 and −4 m s^{-1} with some values as large as −9 m s^{-1}. All five of the dropsondes measured downdraft ventilation below 1 km and some measured ventilation as high as 3 km at the top of the profile.

Dropsonde A measured small to moderate negative θ_e perturbations up to about −5 K below 750 m (Figure 10a) in moderate downward motion (Figure 10f) leading to a layer of downdraft ventilation near the surface (Figure 10k). There was an intense downdraft measured by dropsonde A (Figure 10f) just below 1.5-km height, but the θ_e perturbation was near zero at that location.

Dropsondes B, C, D, and E measured large downdraft ventilation of at least 1 km in depth (Figures 10l–10o). Three of those dropsondes—B, C, and E—measured large negative θ_e perturbations of about −10 K over some layer in the profile (Figures 10b and 10e). The lowest θ_e near the surface was measured by dropsonde C below 1-km height where the θ_e decreased to nearly 350 K (Figure 10c). The θ_e profile measured by dropsonde E also measured θ_e around 350 K between 1–3-km height (Figure 10e). Additionally of note, the downward motion measured by dropsonde D was between −5 and −9 m s^{-1} for almost the entire profile (Figure 10i).

Dropsonde D measured large downdraft ventilation (Figure 10n), even though the θ_e perturbation was not very large (Figure 10d), due to intense downward motion throughout the profile (Figure 10i). Conversely, dropsonde E measured large downdraft ventilation (Figure 10o), even though the downdraft was weaker (Figure 10j), since the negative θ_e perturbation was large (Figure 10e). Considering these differences, it is important to examine both components of downdraft ventilation ($w_{\downarrow}$, θ_e') to understand the factors contributing to downdraft ventilation structures.

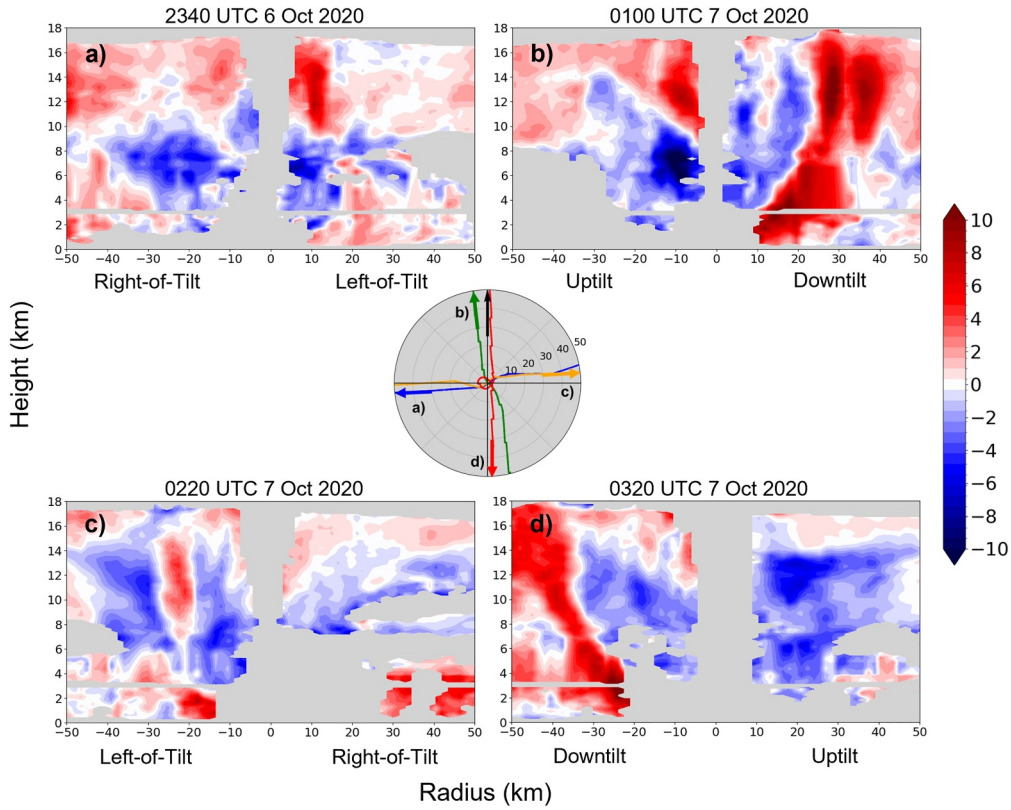

Figure 8. As in Figure 3, but for the second flight from 2230 UTC 6 Oct to 0430 UTC 7 Oct 2020.

Overall, these five dropsondes measured deeper and more negative θ_e perturbations along with deeper downdraft profiles than during the RI period, yielding deeper and more substantial downdraft ventilation signatures, which are consistent with the weakening that Delta experienced. Next, the connection between the downdraft ventilation observations and changes in the TC structure as Delta weakened are examined.

4.2.2. Downdraft Ventilation and the TC Structure

The relationship between the downdraft ventilation and TC structure was explored by comparing the dropsonde observations with the TDR reflectivity and vertical wind (Figure 11). Compared to the RI period, the TC structure had degraded. Unlike during the RI period, the inner-core deep convection was not symmetric about the eye and

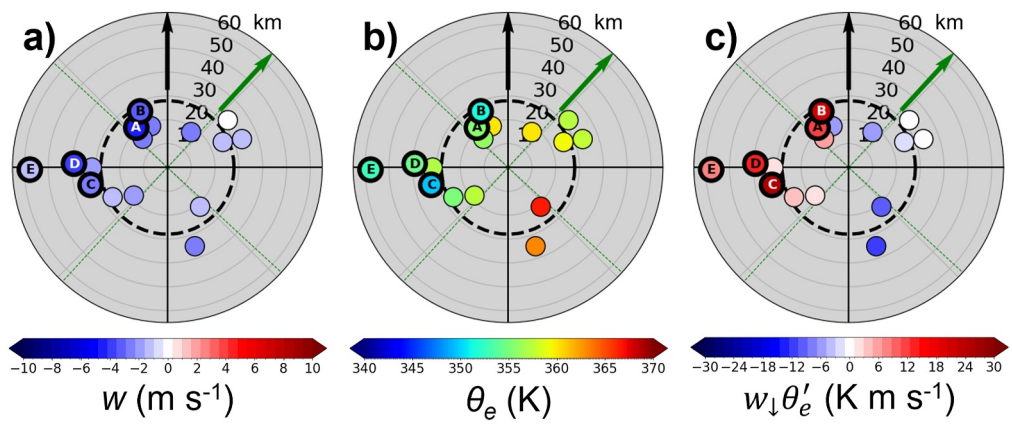

Figure 9. As in Figure 4, but for the second flight from 2230 UTC 6 Oct to 0430 UTC 7 Oct 2020.

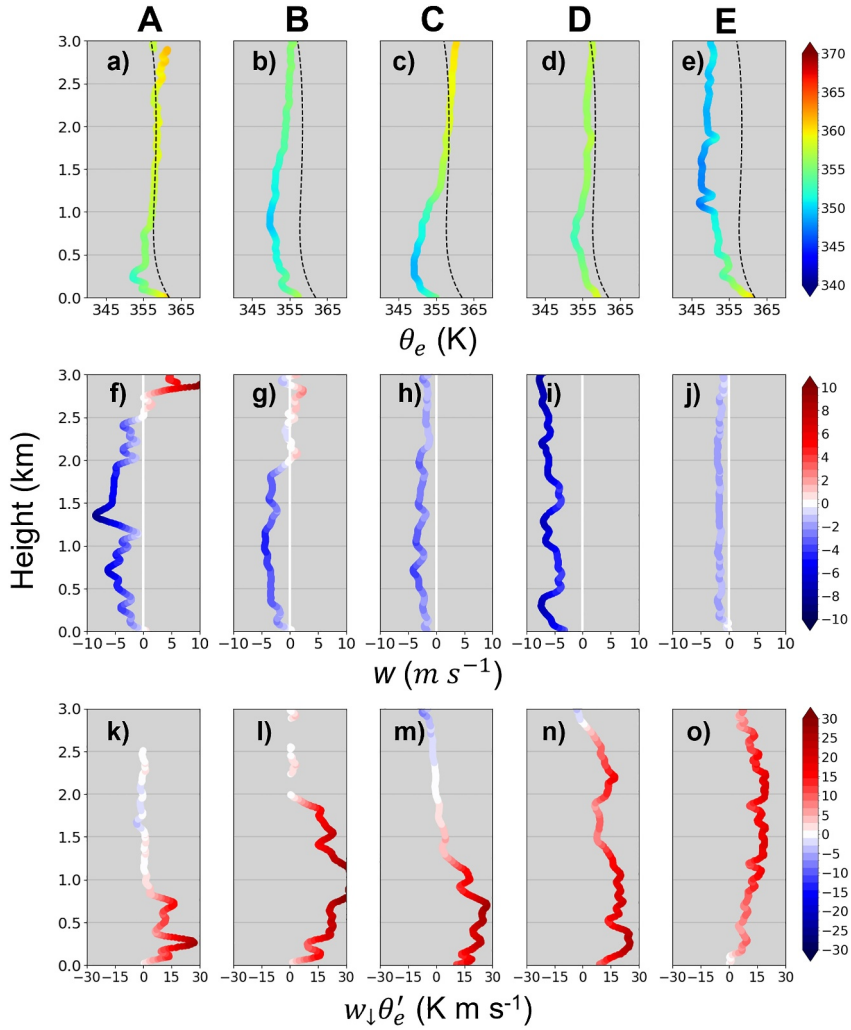

Figure 10. As in Figure 5, but for the second flight from 2230 UTC 6 Oct to 0430 UTC 7 Oct 2020.

was, instead, limited to the downtilt and left-of-tilt semicircles where the precipitation features were primarily located. Furthermore, over the period measured by the three passes, it appears that the radius of the eye increased from about 10 km during the first pass (Figure 11a) to about 20 km (Figure 11c) during the last pass, as deduced by the area with minimal scatterers near the center. All the downdraft ventilation measured during these three passes was in moderate to deep convective precipitation (Figure 12).

Dropsonde A was located downtilt on the upwind side of large reflectivity values around 40 dBZ just inside the RMW between the 20 and 22 km radii (Figure 11a). This dropsonde was likely launched within the eyewall since it was collocated with large reflectivity and windspeeds just below the TC's maximum wind (not shown). There were also positive θ_e perturbations and updrafts above 2.5 km (Figures 10a and 10f). Below 2.5 km, the dropsonde measured downdrafts all the way to the surface (Figure 10f). This updraft–downdraft transition could indicate a downdraft below a sloped eyewall updraft. Then, below 750 m, the dropsonde measured negative θ_e perturbations (Figure 10a) and downdraft ventilation (Figure 10k).

Dropsonde B was located downtilt just outside the eyewall on the inner edge of the RMW between the 25 and 29 km radii (Figure 11a). The dropsonde measured low θ_e and moderately intense downdrafts for much of the profile (Figures 10b and 10g). The difference in θ_e between dropsondes A and B, which were only 5–10 km apart, was between 5 and 10 K above 500-m height (Figures 10a and 10b). Such a large difference shows how low-θ_e air was proximal to the eyewall. The downdraft ventilation measured by dropsondes A and B close to the TC center,

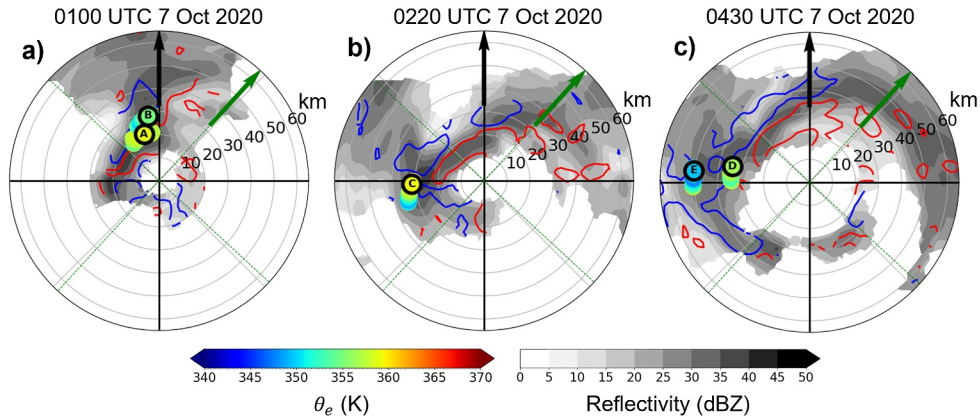

Figure 11. As in Figure 6, but for the second flight from 2230 UTC 6 Oct to 0430 UTC 7 Oct 2020.

and in the downtilt convection, could stunt the development of new convection and limit the extent of strong upward motions, thus weakening the TC (Alland et al., 2021a).

Dropsondes C and D, shown in Figures 11b and 11c, were located left-of-tilt outside the RMW between the 30 and 40 km radii, and were downwind of moderate reflectivity (~35 dBZ) and updrafts. As precipitation from the downtilt convection circulated downwind to the left-of-tilt side where upward motion ceased, the precipitation fell into relatively low-θ_e air, causing evaporative cooling and descent into the boundary layer. Dropsonde E, which measured low θ_e (~350 K) for much of the profile, was located left-of-tilt at a radius of about 56 km, 2x the RMW, and near the interface of convective and stratiform precipitation (Figures 11c and 12c).

Considering the analysis of all the dropsondes during flight 2, low-θ_e air, intense downdrafts, and downdraft ventilation were prevalent in Delta. The downdraft ventilation was located within 2x the RMW downtilt and left-of-tilt where much of the convection in the TC was occurring. These results point to the degradation of the inner-core structure, suppression of convection, and the overall weakening of the storm.

5. Investigation of the Deep Intense Downdrafts

The deep, intense downdrafts measured during the RI period sampled by the first flight were examined in more detail to determine potential causes. The vertical motion asymmetry in Delta's eyewall during the first flight, highlighted by deep, intense downdrafts, was surprising since the storm was still undergoing RI. These downdrafts were examined in more detail to consider potential causes and explore how they affect the stability profiles. In a tilted vortex, vertical descent is required left-of-tilt to maintain thermal wind balance (Jones, 1995). This adiabatic descent (on the order of 0.1 m s^{-1}) alone would not result in downdrafts as strong as those observed in

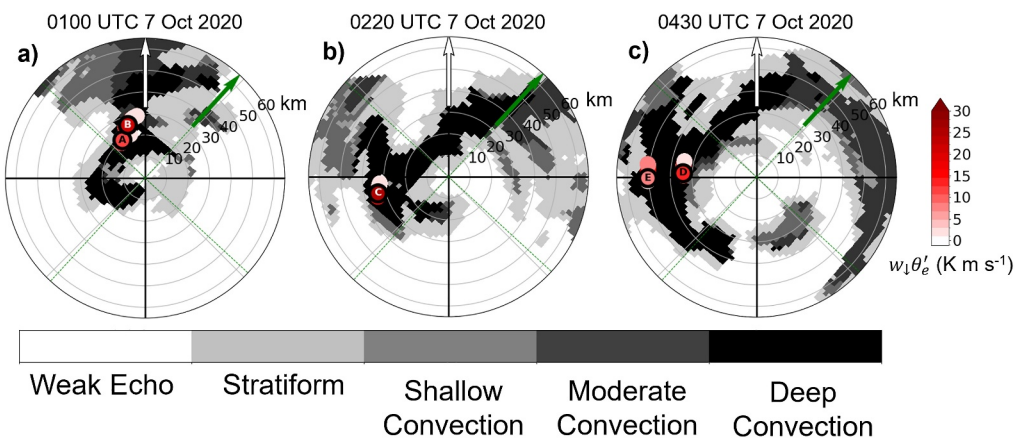

Figure 12. As in Figure 7, but for the second flight from 2230 UTC 6 Oct to 0430 UTC 7 Oct 2020.

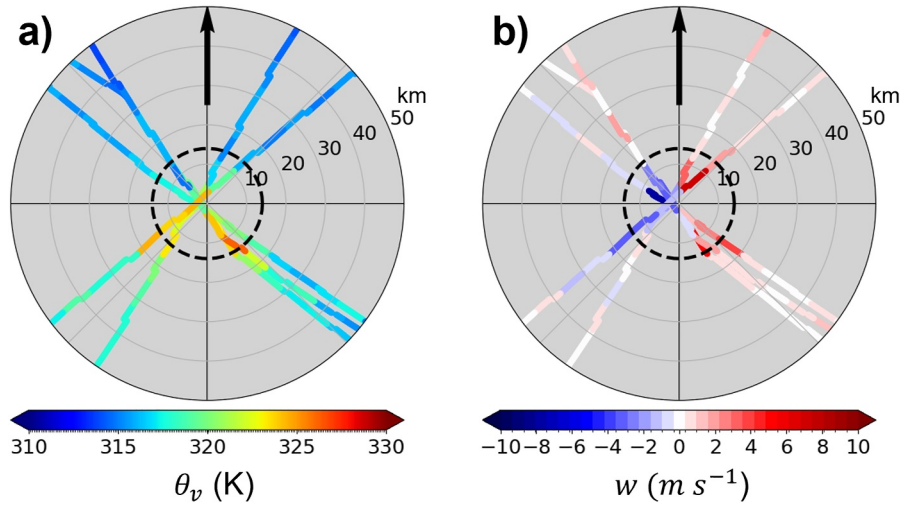

Figure 13. (a) Flight-level θ_v (K) and (b) vertical wind $\left(\text{m s}^{-1}\right)$ for each center pass through Hurricane Delta (2020) from 1030 to 1700 UTC 6 Oct 2020. Flight-level data is smoothed from 1-s to 1-min resolution. The black arrow indicates the vortex tilt direction. The dashed back circle marks the RMW.

Delta. Therefore, diabatic effects, such as sublimation and evaporation, would be necessary to enhance the downdrafts via the production of negative buoyancy.

The flight-level virtual potential temperature (θ_v) was examined as a proxy for buoyancy (AMS Glossary). Anomalously low θ_v is indicative of negative buoyancy, whereas anomalously high θ_v is indicative of positive buoyancy. In all the center passes during the flight, there was no clear relationship between θ_v magnitude and updrafts/downdrafts (Figure 13). Sometimes, low θ_v coincided with downdrafts; however, sometimes updrafts also had low θ_v or downdrafts had large θ_v. Perturbations of θ_v are associated with vertical accelerations and not vertical velocity directly, which could explain the lack of a direct relationship between θ_v and downdrafts. A wavenumber-1 asymmetry existed in the flight-level θ_v (Figure 13a) where higher θ_v was located uptilt and lower θ_v was located downtilt. A similar asymmetry was present in the flight-level vertical velocity (Figure 13b) where downdrafts were located left-of-tilt and updrafts were primarily located right-of-tilt, consistent with TDR observations (Figure 6). There could be other complicating factors affecting the vertical velocity that these observations alone cannot explain, such as dynamical pressure perturbations.

One possible explanation for downdrafts coinciding with large θ_v is that the downdrafts were overshooting their level of neutral buoyancy, which would produce "onion-like" shapes in the temperature and dewpoint profiles (Zipser, 1977). The onion shape of the profiles represents layers of convective inhibition (i.e., thermal inversion layers) to parcels below (Nguyen et al., 2019). The inversion layers suppress convection and prevent updrafts from growing. Those layers would need to be lifted, presumably on the right-of-tilt side of the TC, before deep convection could occur (Nguyen et al., 2019).

Dropsondes F and E from flight 1 (Figure 4) were located outside the eye in deep, intense downdrafts and had onion shaped profiles (Figure 14). Dropsonde F (Figure 14a) had a dry and warm layer between the top of the profile (700 hPa) and 750 hPa with a relative humidity of ∼35% and a maximum temperature of ∼28°C. This dry and warm air resulted in large θ_v magnitudes in the layer. The large θ_v coincided with an intense, unsaturated downdraft with values around -10 m s^{-1}. The downdraft quickly weakened near the temperature inversion and an updraft was measured below. From a parcel perspective, the anomalously high θ_v located above the inversion indicates positive buoyancy that would decelerate the downdraft and keep it from reaching closer to the surface. The inversion would also cap any updrafts below in the lower levels. Dropsonde E (Figure 14b) measured three inversion layers with the lower two (indicated in the figure) encapsulating an intense downdraft in an unsaturated region. This downdraft coincided with lower θ_v than the previous sounding. The downdraft weakened at the lowest inversion at 900 hPa.

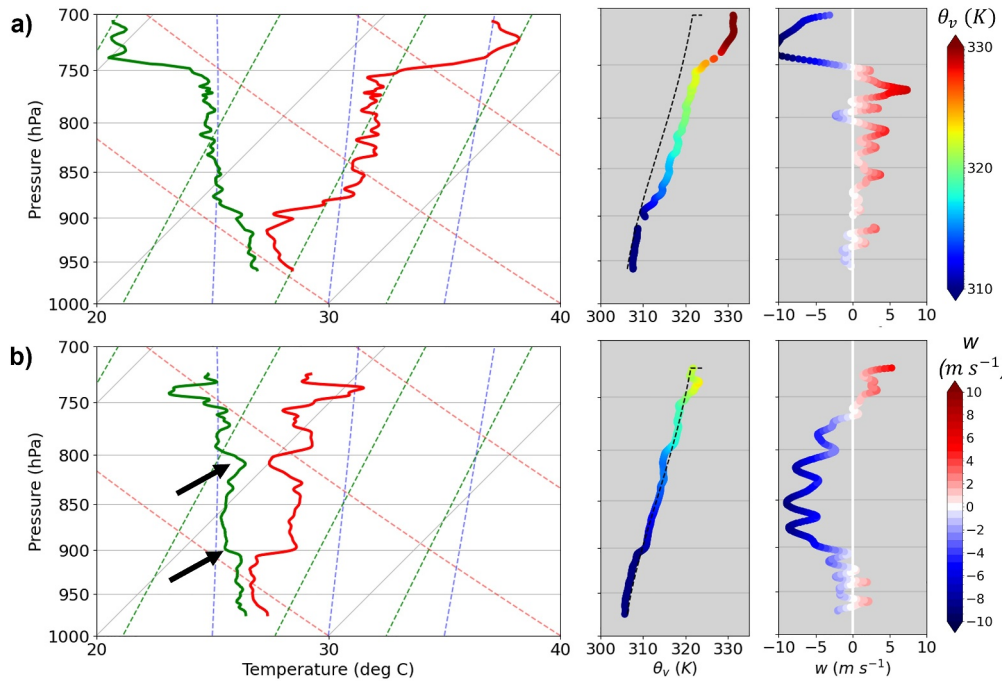

Figure 14. Sounding analysis for (a) dropsonde F and (b) dropsonde E from flight 1 (Figure 4) that were launched in downdrafts in Hurricane Delta during RI. The left column shows skewT diagrams of temperature (°C, red) and dewpoint (°C, green) profiles. The middle column is the θ_v profile (shading) and mean θ_v of the inner core dropsondes (dashed line). The right column is the vertical wind profile (shading) and the white line marks 0 m s^{-1}. Black arrows indicate two inversion layers in the sounding profile.

Determining the cause of the intense, deep downdrafts is challenging with observations, in part because the diabatic heating cannot be directly measured with the aircraft instruments. Further examination using numerical modeling simulations of Delta would be required to study the extent to which diabatic processes influence the downdrafts. Additionally, a modeling study would provide the opportunity to perform a trajectory analysis to find where the low-θ_e air originates and how far the downdrafts transport this air toward the surface.

Wadler et al. (2021) performed idealized simulations to study the thermodynamic characteristics of downdrafts in two TCs of different intensities. The downdrafts in their simulations were not as deep or intense as those observed in Delta; however, idealized experiments similar to theirs could be used to study deep, intense downdrafts. A real-case modeling study was performed by Alland and Davis (2022) to study ventilation in Hurricane Michael (2018). Their results showed downdraft ventilation that was weaker than what was observed in Delta. A similar real-case modeling study of Delta could be performed to study its downdrafts. Ideally, the simulation would need to capture Delta's compact structure and rapid intensification, along with the intense, deep downdrafts. The Hurricane Analysis and Forecast System configuration B (HAFS-B) operational model simulated deep, moderately intense downdrafts in Delta near the TC's peak intensity (AOML Hurricane Model Viewer, n.d.). Additionally, a simulation of Delta from the Coupled Ocean-Atmosphere Mesoscale Prediction System-Tropical Cyclones (COAMPS-TC) model captured intense, moderately deep downdrafts along with the rapid intensification and subsequent rapid weakening (not shown). Examining these simulations is beyond the scope of the current observational study, but these simulations could be used to study the downdrafts in Delta in more detail in follow-on research.

6. Discussion and Conclusion

Hurricane Delta's weakening was abrupt and initially unexpected since the TC appeared to be in a favorable environment prior to making landfall. Toward the end of a period of RI, as Delta was approaching the Yucatán Peninsula, the vertical wind shear increased causing the compact vortex to tilt. The tilted vortex exposed the TC inner core to ventilation and likely initiated intense, deep downdrafts. As eyewall convection diminished, the

extreme rapid intensification halted and the TC began rapidly weakening. Downdraft ventilation of low-θ_e air was observed in the TC inner core and likely contributed to weakening the TC before it made landfall.

In this study, two consecutive NOAA P-3 reconnaissance flights into Delta were examined during the RI and rapid weakening periods, respectively. The analysis of the TC structure and thermodynamics from observations made by the TDR and dropsondes yielded evidence of possible causes for Delta's abrupt weakening, which are compared with results from previous modeling and observational studies next.

During the RI period, deep convection was mostly symmetric around the TC center. This symmetry decreased during the weakening period where deep convection was primarily located downtilt and left-of-shear. During the weakening period, little TDR reflectivity was present uptilt, indicating minimal precipitation there. This precipitation asymmetry is consistent with previous studies (e.g., Rios-Berrios et al., 2024).

The intense, deep downdrafts observed toward the end of RI were primarily located left-of-tilt, which is consistent with the results of the modeling experiments conducted by Alland et al. (2021a). The downdrafts observed in Delta had similar depth and intensity to those described in the observational studies of R. A. Black et al. (1994) and M. L. Black et al. (2002). Due to their intensity, the downdrafts were likely caused by diabatic processes; however, these processes could not be measured directly from the aircraft observations. The azimuthal location of the updrafts and downdrafts during Delta's RI resembled the updraft–downdraft couplet described by R. A. Black et al. (1994) and M. L. Black et al. (2002) where deep updrafts were located directly across the eye from deep downdrafts. Interestingly, the updraft-downdraft couplet appeared before the start of the weakening period.

Despite the intense downdrafts during the RI period, weakening did not immediately occur. Little downdraft ventilation was observed since θ_e was mostly symmetric and relatively large around the TC center. The strongest evidence of downdraft ventilation during the RI period was during the last center pass of flight 1 that occurred about 1.5 hr before Delta reached peak intensity. The lack of downdraft ventilation during the RI period was perhaps why the TC had not started weakening. Although the downdraft ventilation in Delta during the 12 hr between the two sampling periods cannot be determined due to the lack of aircraft observations, the increased downdraft ventilation toward the end of the first flight, with the largest magnitude observed shortly before peak intensity, suggests the early formation of downdraft ventilation that contributed to the eventual weakening of Delta.

During the weakening period, sampled by the second flight, more widespread downdraft ventilation was observed. The θ_e observations showed a greater azimuthal asymmetry than during the RI period where lower θ_e was located left-of-tilt and left-of-shear. The location of the downdraft ventilation relative to the tilt and shear directions is consistent with the results of modeling studies of downdraft ventilation (Alland et al., 2021a). Downdraft ventilation occurring near the end of RI as the vertical wind shear and vortex tilt increased corresponds with the results from Finocchio and Rios-Berrios (2021), who showed a similar sequence of events in their idealized modeling experiments. The observed downdraft ventilation is a likely cause of Delta's weakening where the low-θ_e air transported to the near-surface could dilute the high-θ_e boundary layer air in the inner core (Alland et al., 2021a; Powell, 1990; Riemer et al., 2010, 2013; Wadler et al., 2021; Yu et al., 2023; Zhang et al., 2013). Further suggesting that downdraft ventilation likely caused Delta's weakening, some of the more prevalent causes for TC weakening, such as colder sea surface temperatures and eyewall replacement cycles, were not observed during and prior to Delta's weakening (Cangialosi & Berg, 2021).

The downdraft ventilation observed during both flights was primarily located in convective precipitation pointing to the likelihood that the downdrafts transporting the low-θ_e air were caused by diabatic processes, such as evaporative cooling. Some of the dropsondes that measured downdraft ventilation were located at the interface between convective and stratiform precipitation. It is possible that this interface is a favorable location for downdraft ventilation due to the transition in vertical velocity profiles between the two regimes and the enhancement of evaporatively cooled downdrafts in the lower troposphere that may result (Didlake & Houze, 2009).

The ability of the downdraft ventilation to weaken Delta was enhanced by its location in the left-of-tilt, and left-of-shear, semicircles. The motion of Delta was generally northwestward, and the shear direction was easterly. In a shear-relative perspective, the northwestward storm motion would enhance the surface winds and heat fluxes primarily right-of-shear, while reducing them left-of shear (Chen et al., 2019; Lee et al., 2021; Rappin & Nolan, 2012). Weaker surface fluxes left-of-shear, where the downdraft ventilation was located, would result in

reduced recovery of the low-θ_e air. Additionally, the large magnitude of the downdraft ventilation observed during the weakening period was more likely to offset the recovery from surface heat fluxes (Finocchio & Rios-Berrios, 2021). Downdraft ventilation observations during the weakening period were within about 10 km of eyewall updrafts, which Wadler et al. (2021) showed was more conducive for downdraft ventilation to weaken a TC.

This study presents an analysis of downdrafts and downdraft ventilation observed in Hurricane Delta (2020), and how they acted to rapidly weaken the TC. The method for calculating downdraft ventilation requires measurements of vertical motion and θ_e in the TC inner core. Dropsondes from the NOAA P-3 aircraft provide these observations near the TC center but are limited to the lower troposphere ($<\sim$3-km height). In a modeling study, Alland et al. (2021a) found that downdraft ventilation was primarily located in the lower troposphere existing below 3-km height with a maximum near 1 km. Although downdraft ventilation may appear more often in lower levels, the deep downdrafts observed in Delta suggest the possibility that downdraft ventilation may also occur in middle to upper levels consistent with Yu et al. (2023). In future work, we plan to study observations of radial and downdraft ventilation together to explore the three-dimensional pathway of ventilation in TCs and how these pathways vary across TCs at different intensities.

Data Availability Statement

All data sets used in this study are publicly available from their respective sources. TC-RADAR (Fischer et al., 2022), TDR profile (Zhang et al., 2023), and dropsonde data are available from the NOAA Atlantic Oceanographic and Meteorological Laboratory Hurricane Research Division data repository (n.d.) at https://www.aoml.noaa.gov/ftp/hrd/data/. Bias-corrected TDR reflectivity is available from Fischer and Wadler (2023). The Statistical Hurricane Intensity Prediction Scheme (SHIPS) developmental database (n.d.) can be found at https://rammb2.cira.colostate.edu/research/tropical-cyclones/ships/ and the IR satellite data set can be found at Janowiak et al. (2017).

Acknowledgments
The first author was supported by NASA FINESST Fellowship 80NSSC23K1551 and the Naval Research Enterprise Intern Program. The second and third authors were supported by NASA Grant 80NSSC23K1261. We also acknowledge the joint NOAA-ONR field program for the data analyzed in this study, as part of ONR Grants N000142012071 and N000142312443 received by the second author. The fourth author was supported by ONR Grant Program Element 0601153N. We thank three anonymous reviewers for their constructive comments that helped to improve this manuscript.

References

Ahern, K., & Cowan, L. (2018). Minimizing common errors when projecting geospatial data onto a vortex-centered space. *Geophysical Research Letters*, *45*(21). https://doi.org/10.1029/2018GL079953

Alland, J. J., & Davis, C. A. (2022). Effects of surface fluxes on ventilation pathways and the intensification of Hurricane Michael (2018). *Journal of the Atmospheric Sciences*, *79*(4), 1211–1229. https://doi.org/10.1175/JAS-D-21-0166.1

Alland, J. J., Tang, B. H., Corbosiero, K. L., & Bryan, G. H. (2021a). Combined effects of midlevel dry air and vertical wind shear on tropical cyclone development. Part I: Downdraft ventilation. *Journal of the Atmospheric Sciences*, *78*(3), 763–782. https://doi.org/10.1175/JAS-D-20-0054.1

Alland, J. J., Tang, B. H., Corbosiero, K. L., & Bryan, G. H. (2021b). Combined effects of midlevel dry air and vertical wind shear on tropical cyclone development. Part II: Radial ventilation. *Journal of the Atmospheric Sciences*, *78*(3), 783–796. https://doi.org/10.1175/JAS-D-20-0055.1

Alvey, G. R., Fischer, M., Reasor, P., Zawislak, J., & Rogers, R. (2022). Observed processes underlying the favorable vortex repositioning early in the development of Hurricane Dorian (2019). *Monthly Weather Review*, *150*(1), 193–213. https://doi.org/10.1175/MWR-D-21-0069.1

AOML Hurricane Model Viewer. (n.d.). AOML Hurricane Model viewer. Retrieved from https://storm.aoml.noaa.gov/viewer/

Black, M. L., Gamache, J. F., Marks, F. D., Samsury, C. E., & Willoughby, H. E. (2002). Eastern Pacific Hurricanes Jimena of 1991 and Olivia of 1994: The effect of vertical shear on structure and intensity. *Monthly Weather Review*, *130*(9), 2291–2312. https://doi.org/10.1175/1520-0493(2002)130⟨2291:EPHJOA⟩2.0.CO;2

Black, R. A., Bluestein, H. B., & Black, M. L. (1994). Unusually strong vertical motions in a Caribbean hurricane. *Monthly Weather Review*, *122*(12), 2722–2739. https://doi.org/10.1175/1520-0493(1994)122⟨2722:USVMIA⟩2.0.CO;2

Cangialosi, J. P., & Berg, R. (2021). *Hurricane Delta (AL262020)* (p. 46). National Hurricane Center Tropical Cyclone Report. Retrieved from https://www.nhc.noaa.gov/data/tcr/AL262020_Delta.pdf

Chen, B.-F., Davis, C. A., & Kuo, Y.-H. (2019). An idealized numerical study of shear-relative low-level mean flow on tropical cyclone intensity and size. *Journal of the Atmospheric Sciences*, *76*(8), 2309–2334. https://doi.org/10.1175/JAS-D-18-0315.1

Churchill, D. D., & Houze, R. A. (1984). Development and structure of winter monsoon cloud clusters on 10 December 1978. *Journal of the Atmospheric Sciences*, *41*(6), 933–960. https://doi.org/10.1175/1520-0469(1984)041⟨0933:DASOWM⟩2.0.CO;2

Dai, Y., Majumdar, S. J., & Nolan, D. S. (2021). Tropical cyclone resistance to strong environmental shear. *Journal of the Atmospheric Sciences*, *78*(4), 1275–1293. https://doi.org/10.1175/JAS-D-20-0231.1

DeMaria, M., & Kaplan, J. (1994). A Statistical Hurricane Intensity Prediction Scheme (SHIPS) for the Atlantic basin. *Weather and Forecasting*, *9*(2), 209–220. https://doi.org/10.1175/1520-0434(1994)009⟨0209:ASHIPS⟩2.0.CO;2

Didlake, A. C., & Houze, R. A. (2009). Convective-scale downdrafts in the principal rainband of Hurricane Katrina (2005). *Monthly Weather Review*, *137*(10), 3269–3293. https://doi.org/10.1175/2009MWR2827.1

Finocchio, P. M., & Rios-Berrios, R. (2021). The intensity- and size-dependent response of tropical cyclones to increasing vertical wind shear. *Journal of the Atmospheric Sciences*. https://doi.org/10.1175/JAS-D-21-0126.1

Fischer, M. S., Reasor, P. D., Rogers, R. F., & Gamache, J. F. (2022). An analysis of tropical cyclone vortex and convective characteristics in relation to storm intensity using a novel airborne Doppler radar database. *Monthly Weather Review*, *150*(9), 2255–2278. https://doi.org/10.1175/MWR-D-21-0223.1

Fischer, M. S., Reasor, P. D., Tang, B. H., Corbosiero, K. L., Torn, R. D., & Chen, X. (2023). A tale of two vortex evolutions: Using a high-resolution ensemble to assess the impacts of ventilation on a tropical cyclone rapid intensification event. *Monthly Weather Review*, *151*(1), 297–320. https://doi.org/10.1175/MWR-D-22-0037.1

Fischer, M. S., & Wadler, J. B. (2023). TC-RADAR v3j data files [Dataset]. *Zenodo*. https://doi.org/10.5281/zenodo.8215173

Franklin, J. L., Black, M. L., & Valde, K. (2003). GPS dropwindsonde wind profiles in hurricanes and their operational implications. *Weather and Forecasting*, *18*(1), 32–44. https://doi.org/10.1175/1520-0434(2003)018⟨0032:GDWPIH⟩2.0.CO;2

Gamache, J. F. (1997). Evaluation of a fully three-dimensional variational Doppler analysis technique. In *Conference on radar meteorology, 28 th, Austin, TX* (pp. 422–423).

Gao, J., Xue, M., Shapiro, A., & Droegemeier, K. K. (1999). A variational method for the analysis of three-dimensional wind fields from two Doppler radars. *Monthly Weather Review*, *127*(9), 2128–2142. https://doi.org/10.1175/1520-0493(1999)127⟨2128:AVMFTA⟩2.0.CO;2

Gu, J.-F., Tan, Z.-M., & Qiu, X. (2015). Effects of vertical wind shear on inner-core thermodynamics of an idealized simulated tropical cyclone. *Journal of the Atmospheric Sciences*, *72*(2), 511–530. https://doi.org/10.1175/JAS-D-14-0050.1

Hoskins, B. J., McIntyre, M. E., & Robertson, A. W. (1985). On the use and significance of isentropic potential vorticity maps. *Quarterly Journal of the Royal Meteorological Society*, *111*(470), 877–946. https://doi.org/10.1002/qj.49711147002

Janowiak, J., Joyce, B., & Xie, P. (2017). NCEP/CPC L3 half hourly 4km global (60S–60N) merged IR V1. Edited by Andrey Savtchenko, Greenbelt, MD [Dataset]. *Goddard Earth Sciences Data and Information Services Center (GES DISC)*. https://doi.org/10.5067/P4HZB9N27EKU

Jones, S. C. (1995). The evolution of vortices in vertical shear. I: Initially Barotropic vortices. *Quarterly Journal of the Royal Meteorological Society*, *121*(524), 821–851. https://doi.org/10.1002/qj.49712152406

Lee, T.-Y., Wu, C.-C., & Rios-Berrios, R. (2021). The role of low-level flow direction on tropical cyclone intensity changes in a moderate-sheared environment. *Journal of the Atmospheric Sciences*, *78*(9), 2859–2877. https://doi.org/10.1175/JAS-D-20-0360.1

Lorsolo, S., Zhang, J. A., Marks, F., & Gamache, J. (2010). Estimation and mapping of hurricane turbulent energy using airborne Doppler measurements. *Monthly Weather Review*, *138*(9), 3656–3670. https://doi.org/10.1175/2010MWR3183.1

Nguyen, L. T., & Molinari, J. (2012). Rapid intensification of a sheared, fast-moving hurricane over the Gulf Stream. *Monthly Weather Review*, *140*(10), 3361–3378. https://doi.org/10.1175/MWR-D-11-00293.1

Nguyen, L. T., Rogers, R., Zawislak, J., & Zhang, J. A. (2019). Assessing the influence of convective downdrafts and surface enthalpy fluxes on tropical cyclone intensity change in moderate vertical wind shear. *Monthly Weather Review*, *147*(10), 3519–3534. https://doi.org/10.1175/MWR-D-18-0461.1

Nguyen, L. T., Rogers, R. F., & Reasor, P. D. (2017). Thermodynamic and kinematic influences on precipitation symmetry in sheared tropical cyclones: Bertha and Cristobal (2014). *Monthly Weather Review*, *145*(11), 4423–4446. https://doi.org/10.1175/MWR-D-17-0073.1

NOAA Atlantic Oceanographic and Meteorological Laboratory Hurricane Research Division. (n.d.). Data repository [Dataset]. *NOAA Atlantic Oceanographic and Meteorological Laboratory Hurricane Research Division*. https://www.aoml.noaa.gov/ftp/hrd/data/

Powell, M. D. (1990). Boundary layer structure and dynamics in outer hurricane rainbands. Part II: Downdraft modification and mixed layer recovery. *Monthly Weather Review*, *118*(4), 918–938. https://doi.org/10.1175/1520-0493(1990)118⟨0918:BLSADI⟩2.0.CO;2

Rappin, E. D., & Nolan, D. S. (2012). The effect of vertical shear orientation on tropical cyclogenesis. *Quarterly Journal of the Royal Meteorological Society*, *138*(665), 1035–1054. https://doi.org/10.1002/qj.977

Reasor, P. D., Eastin, M. D., & Gamache, J. F. (2009). Rapidly intensifying hurricane Guillermo (1997). Part I: Low-Wavenumber structure and evolution. *Monthly Weather Review*, *137*(2), 603–631. https://doi.org/10.1175/2008MWR2487.1

Riemer, M., & Montgomery, M. T. (2011). Simple kinematic models for the environmental interaction of tropical cyclones in vertical wind shear. *Atmospheric Chemistry and Physics*, *11*(17), 9395–9414. https://doi.org/10.5194/acp-11-9395-2011

Riemer, M., Montgomery, M. T., & Nicholls, M. E. (2010). A new paradigm for intensity modification of tropical cyclones: Thermodynamic impact of vertical wind shear on the inflow layer. *Atmospheric Chemistry and Physics*, *10*(7), 3163–3188. https://doi.org/10.5194/acp-10-3163-2010

Riemer, M., Montgomery, M. T., & Nicholls, M. E. (2013). Further examination of the thermodynamic modification of the inflow layer of tropical cyclones by vertical wind shear. *Atmospheric Chemistry and Physics*, *13*(1), 327–346. https://doi.org/10.5194/acp-13-327-2013

Rios-Berrios, R., Davis, C. A., & Torn, R. D. (2018). A hypothesis for the intensification of tropical cyclones under moderate vertical wind shear. *Journal of the Atmospheric Sciences*, *75*(12), 4149–4173. https://doi.org/10.1175/JAS-D-18-0070.1

Rios-Berrios, R., Finocchio, P. M., Alland, J. J., Chen, X., Fischer, M. S., Stevenson, S. N., & Tao, D. (2024). A review of the interactions between tropical cyclones and environmental vertical wind shear. *Journal of the Atmospheric Sciences*, *81*(4), 713–741. https://doi.org/10.1175/JAS-D-23-0022.1

Rios-Berrios, R., & Torn, R. D. (2017). Climatological analysis of tropical cyclone intensity changes under moderate vertical wind shear. *Monthly Weather Review*, *145*(5), 1717–1738. https://doi.org/10.1175/MWR-D-16-0350.1

Rios-Berrios, R., Torn, R. D., & Davis, C. A. (2016a). An ensemble approach to investigate tropical cyclone intensification in sheared environments. Part II: Ophelia (2011). *Journal of the Atmospheric Sciences*, *73*(4), 1555–1575. https://doi.org/10.1175/JAS-D-15-0245.1

Rios-Berrios, R., Torn, R. D., & Davis, C. A. (2016b). An ensemble approach to investigate tropical cyclone intensification in sheared environments. Part I: Katia (2011). *Journal of the Atmospheric Sciences*, *73*(1), 71–93. https://doi.org/10.1175/JAS-D-15-0052.1

Rogers, R. F., Reasor, P. D., Zawislak, J. A., & Nguyen, L. T. (2020). Precipitation processes and vortex alignment during the intensification of a weak tropical cyclone in moderate vertical shear. *Monthly Weather Review*, *148*(5), 1899–1929. https://doi.org/10.1175/MWR-D-19-0315.1

Ryglicki, D. R., Cossuth, J. H., Hodyss, D., & Doyle, J. D. (2018). The unexpected rapid intensification of tropical cyclones in moderate vertical wind shear. Part I: Overview and observations. *Monthly Weather Review*, *146*(11), 3773–3800. https://doi.org/10.1175/MWR-D-18-0020.1

Smith, R. K., & Montgomery, M. T. (2015). Toward clarity on understanding tropical cyclone intensification. *Journal of the Atmospheric Sciences*, *72*(8), 3020–3031. https://doi.org/10.1175/JAS-D-15-0017.1

Statistical Hurricane Intensity Prediction Scheme (SHIPS) developmental database. (n.d.). Statistical Hurricane Intensity Prediction Scheme (SHIPS) developmental database [Dataset]. https://rammb2.cira.colostate.edu/research/tropical-cyclones/ships/

Steiner, M., Houze, R. A., & Yuter, S. E. (1995). Climatological characterization of three-dimensional storm structure from operational radar and rain gauge data. *Journal of Applied Meteorology*, *34*(9), 1978–2007. https://doi.org/10.1175/1520-0450(1995)034⟨1978:CCOTDS⟩2.0.CO;2

Stern, D. P., Bryan, G. H., & Aberson, S. D. (2016). Extreme low-level updrafts and wind speeds measured by dropsondes in tropical cyclones. *Monthly Weather Review*, *144*(6), 2177–2204. https://doi.org/10.1175/MWR-D-15-0313.1

Tang, B. H., & Emanuel, K. (2010). Midlevel ventilation's constraint on tropical cyclone intensity. *Journal of the Atmospheric Sciences*, *67*(6), 1817–1830. https://doi.org/10.1175/2010JAS3318.1

Tang, B. H., & Emanuel, K. (2012a). Sensitivity of tropical cyclone intensity to ventilation in an axisymmetric model. *Journal of the Atmospheric Sciences*. Retrieved from https://dspace.mit.edu/handle/1721.1/77234

Tang, B. H., & Emanuel, K. (2012b). A ventilation index for tropical cyclones. *Bulletin America Meteorology Social*, *93*(12), 1901–1912. https://doi.org/10.1175/BAMS-D-11-00165.1

Tang, B. H., Rios-Berrios, R., Alland, J. J., Berman, J. D., & Corbosiero, K. L. (2016). Sensitivity of axisymmetric tropical cyclone spinup time to dry air aloft. *Journal of the Atmospheric Sciences*, *73*(11), 4269–4287. https://doi.org/10.1175/JAS-D-16-0068.1

Tang, B. H., Rios-Berrios, R., & Zhang, J. A. (2024). Diagnosing radial ventilation in dropsonde observations of Hurricane Sam (2021). *Monthly Weather Review*, *152*(8), 1725–1739. https://doi.org/10.1175/MWR-D-23-0224.1

Tao, C., & Jiang, H. (2015). Distributions of shallow to very deep precipitation–convection in rapidly intensifying tropical cyclones. *Journal of Climate*, *28*(22), 8791–8824. https://doi.org/10.1175/JCLI-D-14-00448.1

Tao, D., & Zhang, F. (2014). Effect of environmental shear, sea-surface temperature, and ambient moisture on the formation and predictability of tropical cyclones: An ensemble-mean perspective. *Journal of Advances in Modeling Earth Systems*, *6*(2), 384–404. https://doi.org/10.1002/2014MS000314

Van Sang, N., Smith, R. K., & Montgomery, M. T. (2008). Tropical-cyclone intensification and predictability in three dimensions. *Quarterly Journal of the Royal Meteorological Society*, *134*(632), 563–582. https://doi.org/10.1002/qj.235

Wadler, J. B., Cione, J. J., Rogers, R. F., & Fischer, M. S. (2023). On the distribution of convective and stratiform precipitation in tropical cyclones from airborne Doppler radar and its relationship to intensity change and environmental wind shear direction. *Monthly Weather Review*, *151*(12), 3209–3233. https://doi.org/10.1175/MWR-D-23-0048.1

Wadler, J. B., Nolan, D. S., Zhang, J. A., & Shay, L. K. (2021). Thermodynamic characteristics of downdrafts in tropical cyclones as seen in idealized simulations of different intensities. *Journal of the Atmospheric Sciences*, *78*(11), 3503–3524. https://doi.org/10.1175/JAS-D-21-0006.1

Wadler, J. B., Zhang, J. A., Jaimes, B., & Shay, L. K. (2018). Downdrafts and the evolution of boundary layer thermodynamics in Hurricane Earl (2010) before and during rapid intensification. *Monthly Weather Review*, *146*(11), 3545–3565. https://doi.org/10.1175/MWR-D-18-0090.1

Wang, J., Bian, J., Brown, W. O., Cole, H., Grubišić, V., & Young, K. (2009). Vertical air motion from T-REX radiosonde and dropsonde data. *Journal of Atmospheric and Oceanic Technology*, *26*(5), 928–942. https://doi.org/10.1175/2008JTECHA1240.1

Willoughby, H. E., & Chelmow, M. B. (1982). Objective determination of hurricane tracks from aircraft observations. *Monthly Weather Review*, *110*(9), 1298–1305. https://doi.org/10.1175/1520-0493(1982)110⟨1298:ODOHTF⟩2.0.CO;2

Yu, C.-L., Tang, B. H., & Fovell, R. G. (2023). Diverging behaviors of simulated tropical cyclones in moderate vertical wind shear. *Journal of the Atmospheric Sciences*, *80*(12), 2837–2860. https://doi.org/10.1175/JAS-D-23-0048.1

Yuter, S. E., & Houze, R. A. (1997). Measurements of raindrop size distributions over the Pacific warm pool and implications for Z–R relations. *Journal of Applied Meteorology*, *36*(7), 847–867. https://doi.org/10.1175/1520-0450(1997)036⟨0847:MORSDO⟩2.0.CO;2

Zawislak, J., Jiang, H., Alvey, G. R., Zipser, E. J., Rogers, R. F., Zhang, J. A., & Stevenson, S. N. (2016). Observations of the structure and evolution of Hurricane Edouard (2014) during intensity change. Part I: Relationship between the thermodynamic structure and precipitation. *Monthly Weather Review*, *144*(9), 3333–3354. https://doi.org/10.1175/MWR-D-16-0018.1

Zhang, J. A., Rogers, R. F., Reasor, P. D., & Gamache, J. (2023). The mean kinematic structure of the tropical cyclone boundary layer and its relationship to intensity change. *Monthly Weather Review*, *151*(1), 63–84. https://doi.org/10.1175/MWR-D-21-0335.1

Zhang, J. A., Rogers, R. F., Reasor, P. D., Uhlhorn, E. W., & Marks, F. D. (2013). Asymmetric hurricane boundary layer structure from dropsonde composites in relation to the environmental vertical wind shear. *Monthly Weather Review*, *141*(11), 3968–3984. https://doi.org/10.1175/MWR-D-12-00335.1

Zipser, E. J. (1977). Mesoscale and convective–scale downdrafts as distinct components of squall-line structure. *Monthly Weather Review*, *105*(12), 1568–1589. https://doi.org/10.1175/1520-0493(1977)105⟨1568:MACDAD⟩2.0.CO;2